An example in which cells with abnormal mitochondria directly cause tissue damage is seen in the mitochondrial morphologic abnormalities in arteriolar smooth muscle cells. Patients 1, 4, and 7 showed arteriolar hyalinosis without having DM. Earlier reports have shown arteriolar lesions similar to those in our cases.[6,11] Arteriolar hyalinosis in non-DM-associated mitochondrial nephropathy shows arteriolar smooth muscle cells containing marked proliferating mitochondria. This may be a background of mitochondrial abnormality-induced arteriolar changes.

In conclusion, we showed that GSECs in kidney tissue may represent abnormal mitochondrial accumulation, as revealed by the high mutant load using PCR. This suggests that GSECs may become a new diagnostic marker to identify secondary FSGS associated with mitochondrial diseases and that it may be useful in avoiding unnecessary noneffective therapy, such as steroids in FSGS.

ACKNOWLEDGMENTS

The authors thank Dr Makoto Ogura, Kashiwa Hospital, The Jikei University School of Medicine, Dr Kosaku Nitta, Tokyo Women's Medical University, Dr Kenjiro Kimura, Dr Junki Koike, St. Marianna University School of Medicine, Dr Mikiya Fujieda, Kochi University, and Dr Kunimasa Yan, Kyorin University, for providing samples of renal biopsies. We also thank Shigeru Horita, Mayuko Ohno, Tokyo Women's Medical University, and Sachiko Ishii, Kashiwa Hospital, The Jikei University School of Medicine, for their support in pathologic analyses. In addition, we thank Mayuko Kato, National Center of Neurology and Psychiatry, for providing technical support during single-cell PCR analysis.

REFERENCES

1. Adedoyin O, Frank R, Vento S, et al. Cardiac disease in children with primary glomerular disorders—role of focal segmental glomerulosclerosis. *Pediatr Nephrol.* 2004;19:408–412.
2. Au KM, Lau SC, Mak YF, et al. Mitochondrial DNA deletion in a girl with Fanconi's syndrome. *Pediatr Nephrol.* 2007;22:136–140.
3. D'Agati VD. The spectrum of focal segmental glomerulosclerosis: new insights. *Curr Opin Nephrol Hypertens.* 2008;17:271–281.
4. DiMauro S, Bonilla E, Zeviani M, et al. Mitochondrial myopathies. *Ann Neurol.* 1985;17:521–538.
5. Dinour D, Mini S, Polak-Charcon S, et al. Progressive nephropathy associated with mitochondrial tRNA gene mutation. *Clin Nephrol.* 2004;62:149–154.
6. Doleris LM, Hill GS, Chedin P, et al. Focal segmental glomerulosclerosis associated with mitochondrial cytopathy. *Kidney Int.* 2000; 58:1851–1858.
7. Egger J, Lake BD, Wilson J. Mitochondrial cytopathy. A multisystem disorder with ragged red fibres on muscle biopsy. *Arch Dis Child.* 1981;56:741–752.
8. Goto Y, Itami N, Kajii N, et al. Renal tubular involvement mimicking Bartter syndrome in a patient with Kearns-Sayre syndrome. *J Pediatr.* 1990;116:904–910.
9. Goto Y, Nonaka I, Horai S. A new mtDNA mutation associated with mitochondrial myopathy, encephalopathy, lactic acidosis and stroke-like episodes (MELAS). *Biochim Biophys Acta.* 1991; 1097:238–240.
10. Güçer S, Talim B, Aşan E, et al. Focal segmental glomerulosclerosis associated with mitochondrial cytopathy: report of two cases with special emphasis on podocytes. *Pediatr Dev Pathol.* 2005;8: 710–717.
11. Hasegawa H, Matsuoka T, Goto Y, et al. Strongly succinate dehydrogenase-reactive blood vessels in muscles from patients with mitochondrial myopathy, encephalopathy, lactic acidosis, and stroke-like episodes. *Ann Neurol.* 1991;29:601–605.
12. Hotta O, Inoue C, Miyabayashi S, et al. Clinical and pathologic features of focal segmental glomerulosclerosis with mitochondrial tRNALeu (UUR) gene mutation. *Kidney Int.* 2001;59:1236–1243.
13. Kambham N, Markowitz GS, Valeri AM, et al. Obesity-related glomerulopathy: an emerging epidemic. *Kidney Int.* 2001;59: 1498–1509.
14. Löwik MM, Hol FA, Steenbergen EJ, et al. Mitochondrial tRNALeu (UUR) mutation in a patient with steroid-resistant nephrotic syndrome and focal segmental glomerulosclerosis. *Nephrol Dial Transplant.* 2005;20:336–341.
15. Mallick N. Secondary focal glomerulosclerosis not due to HIV. *Nephrol Dial Transplant.* 2003;18(suppl 6):vi64–vi67.
16. Mita S, Tokunaga M, Uyama E, et al. Single muscle fiber analysis of myoclonus epilepsy with ragged-red fibers. *Muscle Nerve.* 1998;21: 490–497.
17. Moraes C, Ricci E, Bonilla E, et al. The mitochondrial tRNA [Leu (UUR)] mutation in mitochondrial encephalomyopathy, lactic acidosis, and stroke-like episodes (MELAS): genetic, biochemical, and morphological correlations in skeletal muscle. *Am J Hum Gene.* 1992;50:934–949.
18. Nakada K, Inoue K, Ono T, et al. Inter-mitochondrial complementation: mitochondria-specific system preventing mice from expression of disease phenotypes by mutant mtDNA. *Nat Med.* 2001;7:934–940.
19. Nagashima T, Kato H, Maguchi S, et al. A mitochondrial encephalo-myo-neuropathy with a nucleotide position 3271 (T-C) point mutation in the mitochondrial DNA. *Neuromuscul Disord.* 2001;11:470–476.
20. Niaudet P, Rotig A. The kidney in mitochondrial cytopathies. *Kidney Int.* 1997;51:1000–1007.
21. Niaudet P, Heidet L, Munnich A, et al. Deletion of the mitochondrial DNA in a case of de Toni-Debré-Fanconi syndrome and Pearson syndrome. *Pediatr Nephrol.* 1994;8:164–168.
22. Solez K, Colvin RB, Racusen LC, et al. Banff '05 Meeting Report: differential diagnosis of chronic allograft injury and elimination of chronic allograft nephropathy ("CAN"). *Am J Transplant.* 2007; 7:518–526.
23. Yamagata K, Muro K, Usui J, et al. Mitochondrial DNA mutations in focal segmental glomerulosclerosis lesions. *J Am Soc Nephrol.* 2002;13:1816–1823.

Genomics 94 (2009) 414–422

Contents lists available at ScienceDirect

Genomics

journal homepage: www.elsevier.com/locate/ygeno

TULIP1 (*RALGAPA1*) haploinsufficiency with brain development delay

Keiko Shimojima [a], Yuta Komoike [a,b], Jun Tohyama [c], Sonoko Takahashi [b], Marco T. Páez [a], Eiji Nakagawa [d], Yuichi Goto [d], Kousaku Ohno [e], Mayu Ohtsu [f], Hirokazu Oguni [g], Makiko Osawa [g], Toru Higashinakagawa [b], Toshiyuki Yamamoto [a,*]

[a] International Research and Educational Institute for Integrated Medical Sciences (IREIIMS), Tokyo Women's Medical University, 8-1 Kawada-cho, Shinjuku-ward, Tokyo, 162-8666, Japan
[b] Department of Biology, School of Education, Waseda University, Tokyo, Japan
[c] Department of Pediatrics, Nishi-Niigata Chuo National Hospital, Niigata, Japan
[d] Department of Mental Retardation and Birth Defect Research, National Institute of Neuroscience, National Center of Neurology and Psychiatry, Tokyo, Japan
[e] Division of Child Neurology, Institute of Neurological Sciences, Faculty of Medicine, Tottori University, Yonago, Japan
[f] Department of Pediatrics, Saiseikai Yokohamashi Nanbu Hospital, Yokohama, Japan
[g] Department of Pediatrics, Tokyo Women's Medical University, Tokyo, Japan

ARTICLE INFO

Article history:
Received 21 March 2009
Accepted 25 August 2009
Available online 3 September 2009

Keywords:
Chromosomal deletion
TULIP1 (RALGAPA1)
Brain
Developmental delay
Epilepsy
Human
Zebrafish

ABSTRACT

A novel microdeletion of 14q13.1q13.3 was identified in a patient with developmental delay and intractable epilepsy. The 2.2-Mb deletion included 15 genes, of which *TULIP1* (approved gene symbol: *RALGAPA1*)was the only gene highly expressed in the brain. Western blotting revealed reduced amount of TULIP1 in cell lysates derived from immortalized lymphocytes of the patient, suggesting the association between *TULIP1* haploinsufficiency and the patient's phenotype, then 140 patients were screened for *TULIP1* mutations and four missense mutations were identified. Although all four missense mutations were common with parents, reduced TULIP1 was observed in the cell lysates with a P297T mutation identified in a conserved region among species. A full-length homolog of human *TULIP1* was identified in zebrafish with 72% identity to human. Tulip1 was highly expressed in zebrafish brain, and knockdown of which resulted in brain developmental delay. Therefore, we suggest that *TULIP1* is a candidate gene for developmental delay.

Submicroscopic chromosomal aberrations are considered to comprise up to 15% of all mutations underlying monogenic diseases [1]. Microarray-based comparative genomic hybridization (aCGH) has accelerated to identify such submicroscopic genomic alterations, and many new microdeletion syndromes have been established [2]. Whereas interstitial deletion of 14q13 is rare and only a few patients have been reported. By use of aCGH analyses, we identified a unique 14q13.1q13.3 microdeletion in a patient with developmental delay and intractable epilepsy. Of the 15 genes identified in the microdeletion region, *TULIP1* (approved gene symbol: *RALGAPA1*)was the only one known to be predominantly expressed in normal brain tissue [3]. To evaluate the contribution of *TULIP1* to the patient's neurological symptoms, zebrafish embryos with morpholino knockdown system was used as a model organism [4]. Our results suggest that *TULIP1* is a candidate gene for developmental delay and epilepsy.

Results

Molecular cytogenetic analyses of 14q13.1q13.3 deletion

For patient 1 (P1), a 2.2-Mb microdeletion of 14q13.1q13.3 (33,462,439//35,694,522) was identified using aCGH (Fig. 1). Two-color fluorescent *in situ* hybridization (FISH) analysis confirmed the deletion of 14q13.1q13.3 by the loss of the RP11-26M6 and RP11-35M15 signals (Fig. 2A). Retrospective evaluation of chromosomal G-banding previously provided normal karyotype showed reasonable finding with loss of white band (Fig. 2B). FISH analysis using the same probes revealed that both parents lacked the deletion (data not shown), which indicated de novo deletion in P1. The final karyotype was arr cgh 14q13.1q13.3(33,462,439-35,694,522) ×1.ish(RP11-557O15+,RP11-26M6−,RP11-35M15−,RP11-81F13+,RP11-112H5+) de novo.

To confirm the biological parent-child relationships, microsatellite marker analysis was performed on P1 family members. The results sufficiently verified the biological relationships in this family (Supplementary Table 1) and revealed that P1 had only one peak of D14S70, which is within the deletion region; this peak was common only with the mother and there was no common peak of D14S70 with

* Corresponding author. Fax: +81 3 3352 3088.
E-mail address: yamamoto@imcir.twmu.ac.jp (T. Yamamoto).

0888-7543/$ - see front matter.
doi:10.1016/j.ygeno.2009.08.015

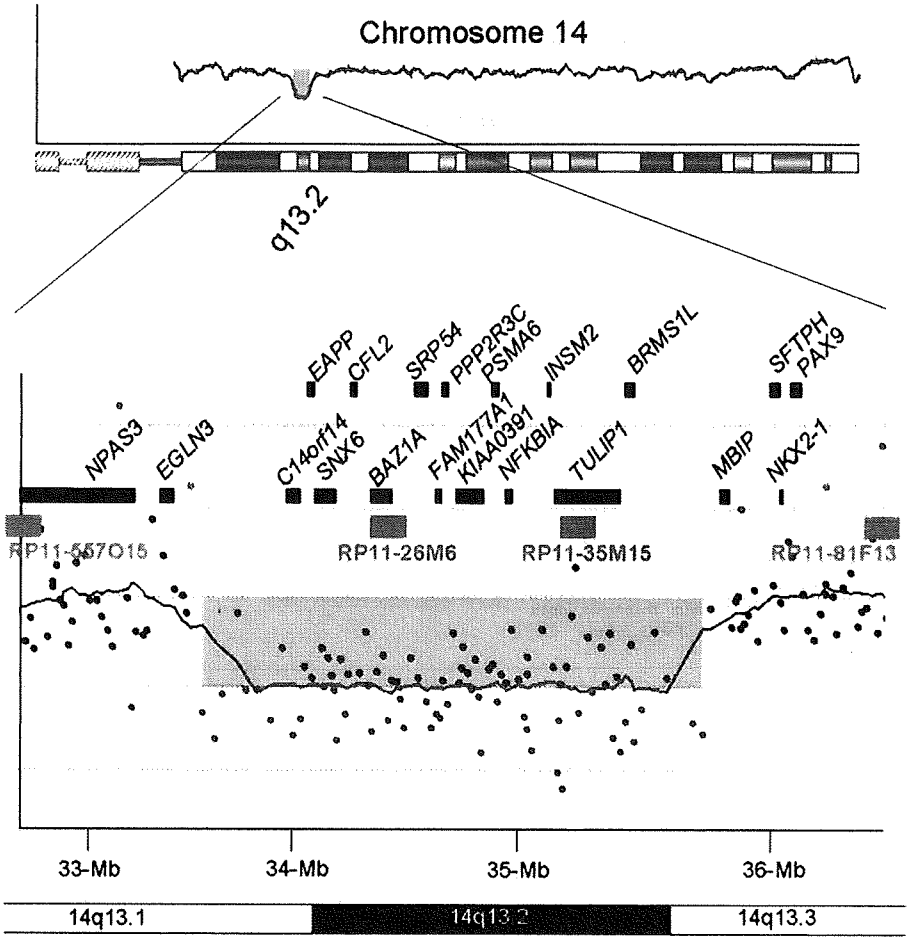

Fig. 1. The result of aCGH showing chromosomal deletion of 14q13.1q13.3 on Chromosome View (upper) and Gene View (bottom). Blue rectangles indicate the region of genomic copy number aberrations. In Gene View, the deletion region was expanded. Axial dimension indicates the physical location on chromosome 14, and vertical dimension indicates $\log_2$ ratio of intensity. Spots indicate the location of probes. Black bars indicate the locations of the known genes. Red and green bars indicate the locations of BAC clones used for FISH analyses. Italic characters indicate gene symbols.

the father (Fig. 2C). These data indicated that the paternally derived allele at this locus was deleted in P1.

Detailed clinical phenotype of P1

At the time of the study, P1 was a 7-year-old girl. Her birth weight was 3038 g and her head circumference at birth was 36 cm; there were no documented neonatal events. At 2 months, she suffered a seizure that continued for a couple of minutes; at that time she opened her eyes and both eyes and arms moved upward and were fixed. Because similar seizures occurred three times during the next 2 h, she was hospitalized. Brain computed tomography (CT) scan and electroencephalography (EEG) revealed no abnormalities. Seizures were refractory to epilepsy medication and occurred a couple of times per day. Similar to West

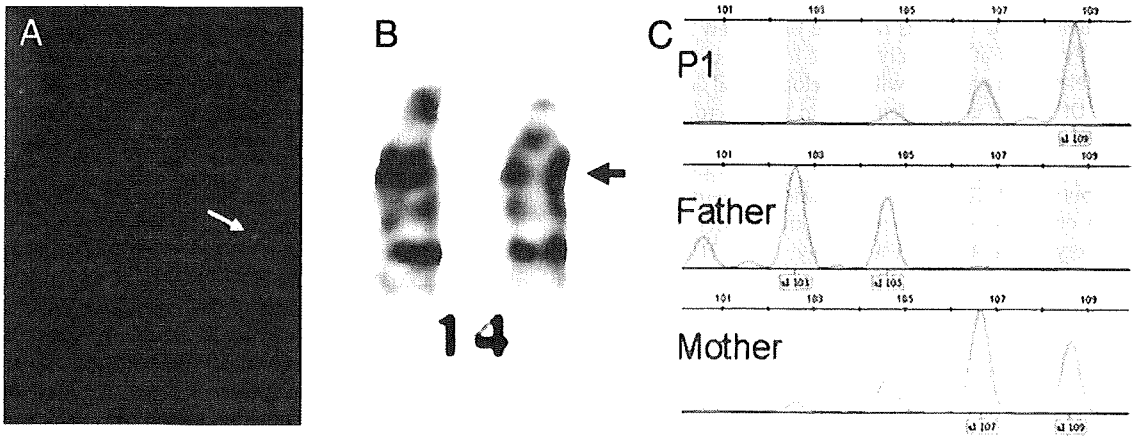

Fig. 2. Molecular cytogenetic analysis of the deletion of 14q13.1q13.3 in P1. (A) FISH analysis using RP11-112H5 (SpectrumOrange) and RP11-35M15 (SpectrumGreen) probes indicated the deletion by the loss of green signal. (B) G-banded chromosome 14 of P1 exhibited deletion of the white band (arrow). (C) GeneMapper analysis of microsatellite marker data indicated that the D14S70 band was only common to P1 and her mother (see also Supplementary Table 1).

syndrome, her seizures were composed of a series of attacks and occurred once a week after the patient reached 3 months of age.

When she was 9 months old, P1 was referred to our institution for treatment of the intractable seizures. There were no dysmorphic features. At that time, she was alert but her reaction to her surroundings was poor. Her eyes could not follow a moving target. Hypotonia was obvious but muscle power was enough to move against gravity. There was no symptom of cranial nerve damage. Tonic convulsions with eye movements and upward movement of the arms were observed intermittently. Blood screening tests, including those for inborn error of metabolism, revealed no abnormalities. The EEG showed a diffuse θ wave and a high voltage θ burst during brief tonic seizures (Supplementary Fig. 1A). However, there were no paroxysmal findings in intermittent phases. Brain magnetic resonance imaging (MRI) showed mild brain atrophy (Supplementary Fig. 1B and C). Brain single photon emission computed tomography (SPECT) showed no areas of hypoperfusion (data not shown). The results from other electrophysiological examinations, including auditory brain response (ABR), visual evoked potential (VEP), somato-sensory evoked potential (SSEP), conduction velocity (MCV), and sensory verve conduction velocity (SCV), were within normal limits (data not shown). Conventional chromosomal examination at 9 months of age indicated a normal female karyotype with 46,XX. At 5 years of age, her developmental level was evaluated using the Enjoji Scale of Infant Analytical Development (ESID) and her developmental quotient was determined to be 32 [5].

TULIP1 screening of additional patients with neurological disorders

Information regarding the genes within the deletion region of P1 was accumulated from the UCSC genome browser (http://www.genome.ucsc.edu/); 15 genes were identified in the 2.8-Mb deleted region (Fig. 1). Among the 15 genes, *TULIP1* was the only gene known to be predominantly expressed in the brain. Thus, *TULIP1* was examined as the candidate gene responsible for the clinical symptoms of P1.

Sequence analysis of the entire coding region of *TULIP1*, which contains 41 exons, was performed using originally accumulated 40 patients' samples and the 100 research resource samples. Four individual missense mutations were identified (Supplementary Fig. 2). Patient 2 (P2) had a c.889C>A nucleotide alteration in exon 9, which is predicted to result in a P297T amino acid substitution. This proband's father had the same alteration. Patient 3 (P3) and his father had a c.1055A>G (D352G) mutation in exon 10. Patient 4 (P4) and her mother had a c.1531G>A (A511T) mutation in exon 12. Patient 5 (P5) and his father had a c.3132T>G (F914C) mutation. Thus, all of the four missense mutations were inherited from healthy parents. Each of the identified missense mutations was negative in 200 normal controls. The entire coding region of *TULIP1* remaining allele of P1 was sequenced and was wild type.

P2 presented with severe mental retardation and intractable epilepsy derived from bilateral perisylvian polymicrogyria. P4 suffered West syndrome in infancy, and manifested intractable epilepsy and moderate mental retardation. P3 and P5 showed moderate mental retardation, but no epilepsy (their family trees are shown in Supplementary Fig. 3).

Analysis of TULIP1 expression

Western blotting using polyclonal rabbit anti-TULIP1 antibody was performed and reduced TULIP1 levels were confirmed in immortalized lymphocytes lysates from P1 and P2 (Fig. 3).

Identification of zebrafish tulip1

In zebrafish, a homolog of human *TULIP1* was previously predicted according to genomic information, but the gene has not yet been

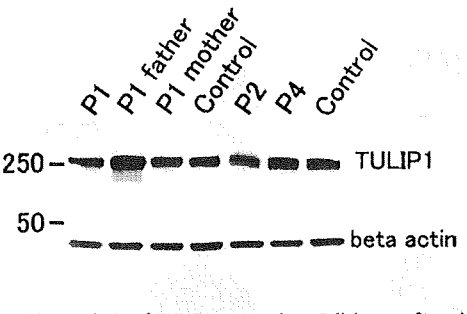

Fig. 3. Western blot analysis of TULIP1 expression. Cell lysates from immortalized lymphocytes derived from the patients indicated at the top were analyzed by Western blotting using a rabbit anti-GARNL1 (TULIP1) polyclonal antibody. P1 and P2 exhibited reduced TULIP1 expression (upper panel). β-Actin levels were evaluated as a control (lower panel).

isolated. Therefore, we cloned and sequenced the cDNA encoding *tulip1* from zebrafish. Using RT-PCR, we identified two splice variants of *tulip1*, *tulip1.1* and *tulip1.2*, which sequences were deposited into GenBank (accession AB476643 and AB476644). The shorter variant (*tulip1.1*) consisted of 6201-bp and encoded a 2066-residue protein, and the longer variant (*tulip1.2*) was 6318-bp and encoded a 2105 residue protein. Information from the zebrafish genomic map revealed that zebrafish *tulip1* was on chromosome 17 and consisted of 41 exons. In addition, two splicing variants were identified based on alternate usage of exon 40. Although the tulip1.2 variant lacks exon 40, this variant is longer than *tulip1.1* because exon 40 contains a stop codon. This exon–intron structure and alternative splicing of exon 40 are common to human and mouse *TULIP1* [3], suggesting that *tulip1* is conserved through vertebrate evolution.

The deduced zebrafish Tulip1.1 and Tulip1.2 protein sequences exhibited 72% identity to the corresponding splicing variants from both human and mouse, and the zebrafish splice variants each contained a Rap/Ran-GAP domain (aa 1848–aa 2027), two putative transmembrane domains (aa 1184–aa1206, aa 1370–aa1392), two putative coiled-coil motifs (aa 10–aa 37, aa 1738–aa 1770) and one leucine zipper motif (aa 1074–aa 1088), all of which are also found in human and mouse TULIP1 proteins at the same positions [3]. Collectively, these results suggested that zebrafish *tulip1.1* and *tulip1.2* are structural and functional homologs of human *TULIP1*.

To carry out *tulip1* knockdown in zebrafish using morpholino antisense oligos, precise 5′ UTR nucleotide sequence information was needed. Thus, we performed 5′ RACE to determine the sequence of the *tulip1* 5′ UTR in our zebrafish strain. Based on the obtained sequence of a 64-nucleotide fragment immediately upstream of the translational initiation site, the residue at the 5′ terminus of this sequence was guanine, whereas the residue of the position in the genomic database was cytosine. This nucleotide alteration was supposed to be the result of m7G 5′ cap structure. Therefore, this fragment means to be a full length of the 5′ UTR.

Spatial expression patterns of tulip1 during zebrafish embryonic development

To determine the spatial expression pattern of *tulip1* in zebrafish, whole-mount *in situ* hybridization of *tulip1* mRNA was performed. At the two-cell stage, *tulip1* mRNA was distributed throughout the two blastomeres (Fig. 4A), indicating that this mRNA was deposited maternally. At the shield stage, after the launch of zygotic gene expression, *tulip1* mRNA was expressed equally in whole blastomeres (Fig. 4B) and this ubiquitous expression pattern was retained during gastrulation and continued until the middle of the segmentation period (Figs. 4C and D). Later in development, distribution of *tulip1* mRNA shifted anteriorly and was restricted to the head region of embryos (Figs. 4E–G), suggesting a role for *tulip1* in zebrafish head development.

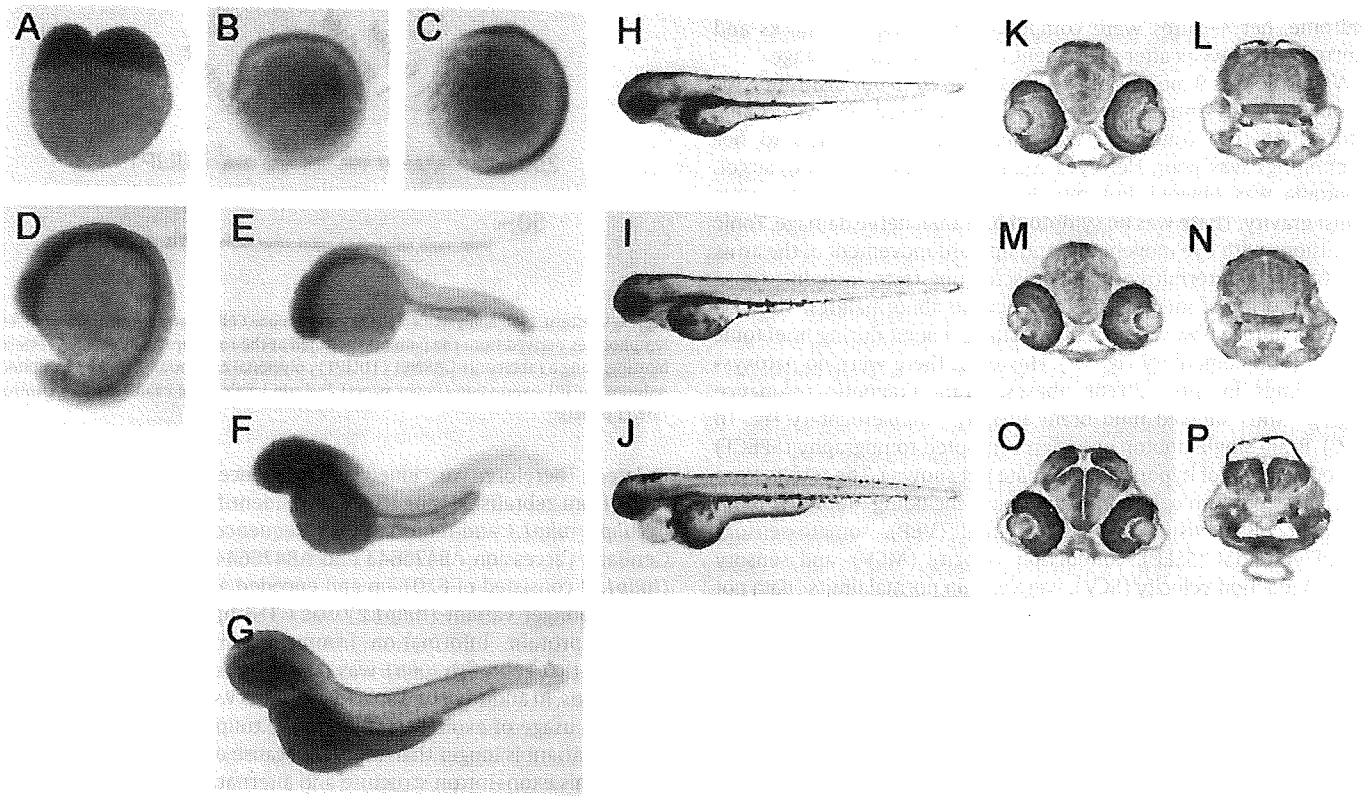

Fig. 4. Expression and functional analyses of *tulip1* in zebrafish. (A–G) *In situ* hybridization of *tulip1* mRNA during development. At the two-cell stage, *tulip1* mRNA was deposited maternally (A) and expressed ubiquitously until the middle of the segmentation period (B, shield stage; C, bud stage; D, 18 somite stage). Distribution of *tulip1* mRNA was shifted anteriorly and restricted in head region of embryos (E, 24 h post-fertilization (hpf); F, 48 hpf; G, 72 hpf). (J, O, P) Knockdown of *tulip1* caused developmental delay of the head and brain. Live whole embryos (H–J) and head cross sections corresponding to the midbrain (K, M, O) and hindbrain (L, N, P) of wild type (H, K, L), control MO-injected (I, M, N) and *tulip1* MO-injected (J, O, P) embryos at 72 hpf. Dorsal is at the top (E–P) and rostral is to the left (E–J).

Gene knockdown of tulip1 causes severe developmental retardation of the brain

To investigate whether *tulip1* is involved in brain development, we performed gene knockdown of *tulip1* in zebrafish using morpholino antisense oligos (MO). At 72 h post-fertilization (hpf), *tulip1* MO1-injected embryos (Fig. 4J) exhibited hypomorphic heads compared to wild type or control MO-injected embryos (Figs. 4H–I), whereas trunk development was relatively normal. In addition, approximately half of all morphants had an enlarged pericardium and increased yolk extension thickness (see representative morphant; Fig. 4J). To investigate whether these defects were caused by the gene-specific knockdown of *tulip1* or not, *tulip1* MO2, which is another morpholino antisense oligo and non-overlapping with *tulip1* MO1, was used. Microinjection of *tulip1* MO2 did not give rise to an enlarged pericardium and rarely caused thickening of the yolk sac (data not shown). Therefore, the heart and the yolk defects are not specific to *tulip1* knockdown. In contrast, *tulip1* MO1 and MO2 caused equivalent growth retardation of the head suggesting that this defect was caused by the specific knockdown of *tulip1* (Figs. 5A and B).

Because the externally hypomorphic head in the zebrafish morphants was similar to the abnormality of the brain observed in P1, serial sections of the head were prepared from *tulip1* MO-injected zebrafish embryos to examine specific brain morphology aberrations. In the normal zebrafish midbrain, the brain ventricle was positioned on the section that crossed the middle of the eyes at 48 hpf (Fig. 5C). This ventricle was obstructed around 60 hpf (Fig. 5E) and completely buried until 72 hpf in wild type (Fig. 4K) and control MO-injected (Fig. 4M) zebrafish. In the normal zebrafish hindbrain, the rhombic lip at 48 hpf was thin and the groove of the medulla oblongata was opened wide (Fig. 5D). The rhombic lip thickened with progressive embryonic development and, as a result, the groove of the medulla oblongata was almost fully occluded at 72 hpf in wild type (Fig. 4L) and control MO-injected (Fig. 4N) zebrafish. In contrast, in *tulip1* MO-injected embryos, the brain ventricle in the midbrain at 72 hpf was unobstructed (Fig. 4O). Similarly, a thin rhombic lip and widely opened groove of the medulla oblongata was observed in the hindbrain at 72 hpf (Fig. 4P). These results indicated that the development of the brain in *tulip1* MO-injected embryos at 72 hpf (Fig. 4O, and P) corresponded to that of the wild type embryo at 48–60 hpf (Figs. 5C–F), and suggested that *tulip1* knockdown results in brain developmental delay by $\geq$12 h (also compare Figs. 5C–D vs. H–I and compare Figs. 4K–L vs. Figs. 5J–K). Whole-body developmental delay was less severe than brain developmental delay; *tulip1* MO-injected embryos at 72 hpf were clearly as progressed as wild type embryos at 60 hpf (Fig. 5G). Collectively, these results indicated that gene knockdown of *tulip1* caused severe and specific brain developmental delay.

Discussion

Using aCGH, we identified a previously uncharacterized chromosomal deletion of 14q13.1q13.3 in a female patient with developmental delay and intractable epilepsy. Familial analysis indicated that the deletion occurred de novo. In the literature, there are at least 19 reported cases with deletions near 14q13, and the deletion identified in the present patient (P1) is the smallest among them (Fig. 6) [6–13]. Clinical findings of available 10 of these previously reported cases are summarized in Table 1. The common manifestations of the 14q13.2 deletion are developmental delay and mild microcephaly (Table 1). In the 2.2-Mb deletion in P1, 15 genes are included according to the 2006 build (Fig. 1).

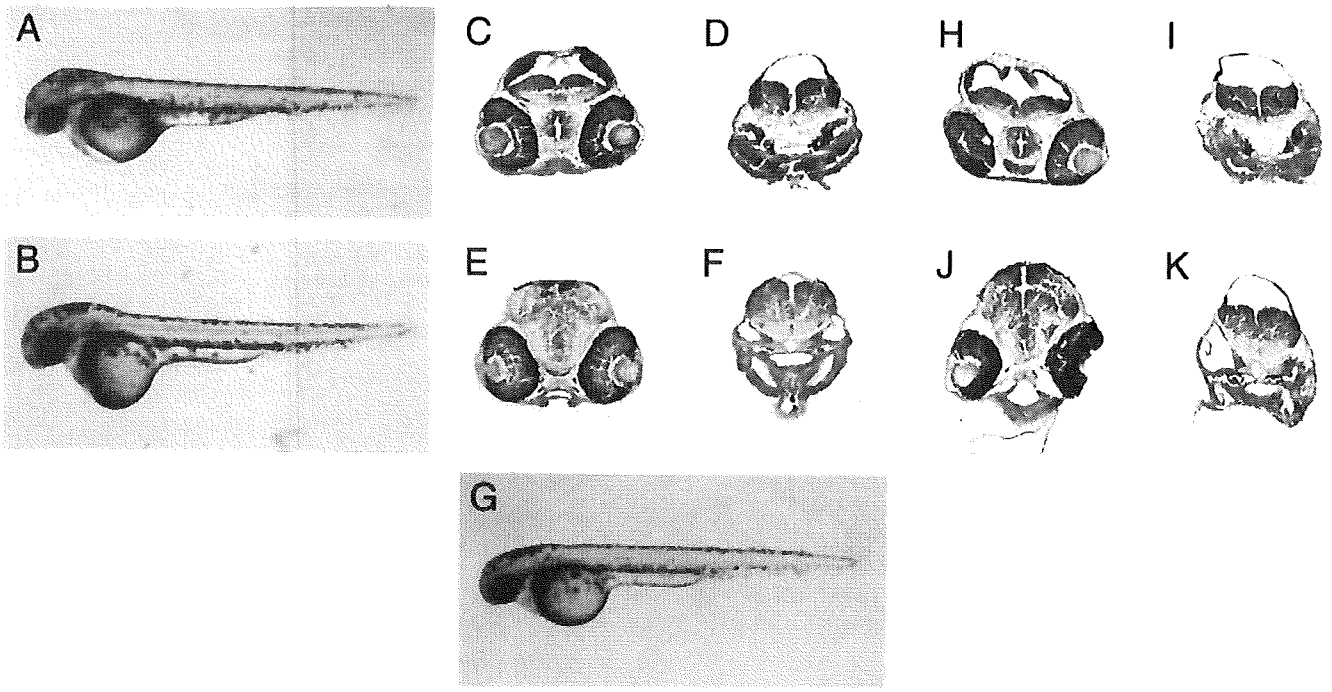

Fig. 5. *tulip1* knockdown analyses of zebrafish. Zebrafish embryos at 48 hpf injected by *tulip1* MO1 (A) and MO2 (B) showed similar hypomorphic head. Cross section of the brain of wild type (C–F) and *tulip1* MO1 embryo (H–K); midbrain (C, E, H, J) and hindbrain (D, F, I, K). Wild type embryos at 48 hpf (C, D) correspond to *tulip1* MO1 embryos at 60 hpf (H, I), and wild type embryos at 60 hpf (E, F) correspond to *tulip1* MO1 embryos at 84 hpf (J, K), which indicate developmental delay. (G) Wild type embryo at 60 hpf.

Schwarzbraun et al. considered *TULIP1* as the candidate gene for the neurological phenotypes of deletion 14q13, and analyzed the genomic structure and the function [3]. According to the study, *TULIP1* was expressed ubiquitously in pre- and postnatal human tissues. The nucleotide sequence of *TULIP1* was predicted to encode Rap–Gap domains [3], which is also contained in *TSC2*, one of the genes responsible for tuberous sclerosis. Since haploinsufficiency of *TSC2* can affects neurological functions [3], Schwarzbraun et al. analyzed the sequence of *TULIP1* in a family with idiopathic basal ganglia calcification (IBGC; Fahr disease), but found no association between

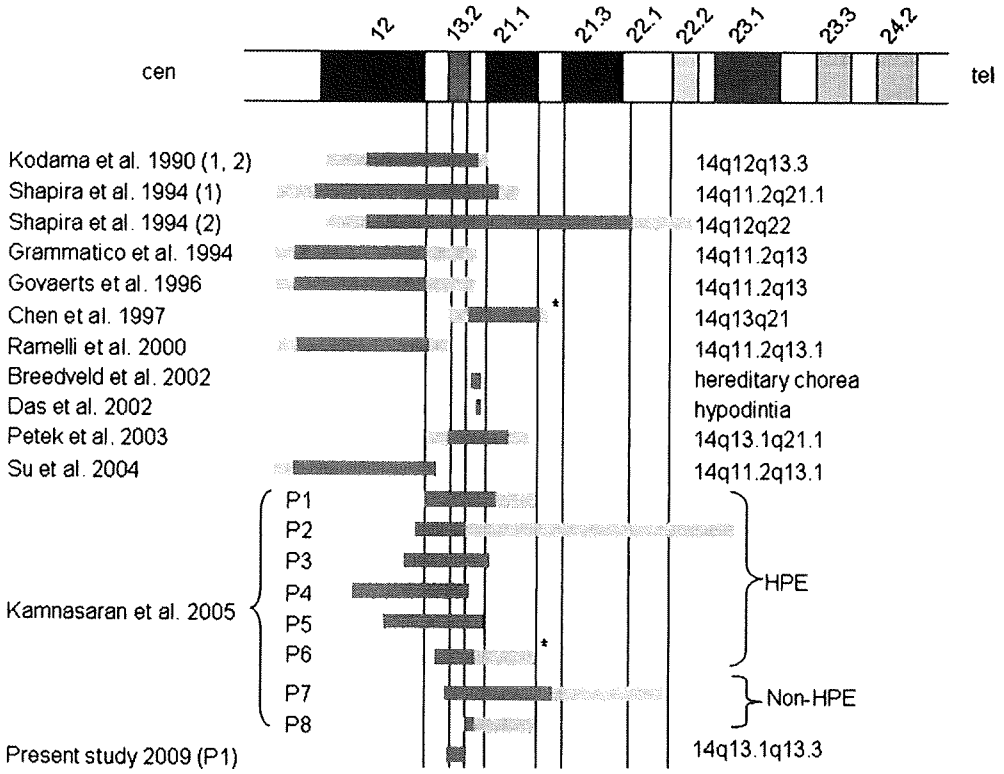

Fig. 6. Chromosome 14 schematic (upper) with the each size of deletions from previously reported patients and P1. Black and gray bars indicate confirmed and suspected deletion regions, respectively. Numbers included in parentheses indicate patient number in the reference manuscripts. Asterisks indicate results derived from the same patient. HPE: holoprosencephaly.

Table 1
Clinical information of the patients having a chromosomal deletion of 14q13q13.

	Kodama et al. 1990 (1) 14q12q13.3	Kodama et al. 1990 (2) 14q12q13.3	Shapira et al. 1994 (1) 14q11.2q21.1	Shapira et al. 1994 (2) 14q12q22	Grammatico et al. 1994 14q11.2q13	Govaerts et al. 1996 14q11.2q13	Chen et al. 1997 14q13q21	Ramelli et al. 2000 14q11.2q13.1	Petek et al. 2003 14q12q13.1	Su et al. 2004 14q11.2q13.1	Present patient 2009 14q13.1q13.3
Origin	mat	mat	pat	pat	NA	pat					pat
Pregnancy											
Oligohydramnion				–	–	–					–
Breech presentation			–		–	–					–
Duration (weeks)	41	41	39	36	38	38		40	40		36
Neonatal period											
Asphyxia		–	–	–	–	–					
Birth length (cm)	49.8	48	48	45.5	52	NA		48	55	49.5	
Birth weight (g)	3150	3150	2455	2345	3270	2370		3300	4435	2700	3038
OFC (cm)	32	32.5	31	32.5	33	30.2		33.5	34	34	36
Congenital anomalies											
Microcephaly											–
Epicanthus			NA		NA						–
Protruding upper jaw				NA	NA						–
Micrognathia					–						–
High narrow palate				NA	NA						–
Cerebral atrophy											
Corpus callosum hypoplasia					NA	–					–
Asymmetric hemisoma			–			–					–
Heart defect			NA		–	–					–
Kidney cysts			NA	NA	NA						NA
Cryptochism	female	female	female	female		–					female
Growth and development											
Growth retardation											–
Feeding problems				NA	NA						–
Arthrogryposis			NA	NA	NA						–
Hip (sub) luxation			NA			NA					–
Eye contact	–		–	–	–	–					–
Spasticity				–							–
Hypostonia			–		–	–					–
Mental retardation											–
Diabetes inspidus			–	–	–						–
Renal tubrular acidosis				–	–	–					–
Reccurent infections				NA	NA						–

mat, maternally derived; pat, paternally derived; NA, not available.

TULIP1 mutation and idiopathic basal ganglia calcification. Whereas, the similarities between *TULIP1* and *TSC2* led us to hypothesize that *TULIP1* might be associated with the idiopathic developmental delay and epilepsy.

In the present study, reduced TULIP1 levels were observed in cell lysates from immortalized lymphocytes derived from P1 (Fig. 3). Subsequent mutation analyses identified no *TULIP1* mutation on the remaining allele. This evidence indicates that *TULIP1* expression is allele-dose dependent, making *TULIP1* a credible candidate gene for the phenotype of P1. We therefore analyzed the entire *TULIP1* coding region from 140 subjects with developmental delay and/or epilepsy. From this second screening, four individual *TULIP1* missense mutations were identified in four patients (Supplementary Fig. 2), and two of them were located within conserved sequence region among mammalian species (Supplementary Fig. 4). However, all four missense mutations were inherited from their healthy parents (Supplementary Figs. 2 and 3).

To confirm whether *TULIP1* deletion influenced the phenotypic appearance of P1, we used a zebrafish knockdown system in which expression of the zebrafish homolog of *TULIP1* was artificially depressed. We first identified and sequenced the full-length cDNA of zebrafish *tulip1* including the 5′ and 3′ UTRs; the zebrafish and human sequences shared 72% identity. *In situ* hybridization revealed that Tulip1 was expressed in the wild type zebrafish forebrain and *tulip1* knockdown resulted in brain developmental delay but normal whole body development. These findings are comparable to that observed for P1, who had *TULIP1* deletion and manifested severe developmental delay, intractable epilepsy, and mild cerebral atrophy.

Kamnasaran et al. reported six patients associated with holoprosencephaly and common 14q13 microdeletion, which is overlapped with that of the present patient (P1) (Fig. 6) [14]. In spite of common deletions, penetrance of holoprosencephaly was not 100%, which may depend on the parental origin of the deletion. Uniparental disomy of chromosome 14 (UPD14) results in a distinctive phenotype with developmental delay and dysmorphic features depending on the parental origin [15,16]. Although the imprinting locus of UPD14 is far from the 14q13 locus, we cannot deny the possibility that penetrance of holoprosencephaly is influenced by the allele origin.

As same as this manner, *TULIP1* may be influenced by genomic imprinting. Although the missense mutation P297T was shared with P2 and her healthy father, western blotting analyses showed reduced TULIP1 expression in immortalized lymphocyte cell extracts from P2. If *TULIP1* was transcribed only from the paternal allele, P2 would only be able to synthesize the mutated protein [17]. The evidence that chromosomal deletion of 14q13.q13.3 in P1 was derived from paternal allele may support this hypothesis. Therefore, we cannot rule out possible pathogenicity of familial missense mutations identified in this study.

Materials and methods

Materials

After informed consent based on the permission of the ethical committee of Tokyo Women's Medical University, peripheral blood samples of 300 patients with idiopathic mental retardation and/or epilepsy of unidentified etiology were accumulated to investigate potential genomic copy number aberrations using aCGH. In some cases of chromosomal aberrations, blood samples were also obtained from both parents of the patient. The samples in which no genomic copy number aberrations were identified were used in the second screening to identify whether gene-specific mutations were present. In this study, 40 samples derived from patients with neurological symptoms including developmental delay and/or epilepsy were used for the second screening. An additional 100 subjects, which were determined by aCGH to be negative for chromosomal aberrations and other known disease-causing mutations, including mutation of *FMR1*, *AFF2*, *PQBP1*, *ARX*, *MECP2*, *ATRX*, *RPS6KA3*, *IL1RAPL1*, *TSPAN7*, *OPHN1*, *PAK3*, *ACSL4*, *AGTH2*, *ARHGEF6*, *GDI1*, *SLC6A8*, *FTSJ1*, *ZNF41*, and *DLG3*, were provided by the consortium of Research Resource for Mental Retardation supported by the Ministry of Welfare, Labor, and Health of Japan [18]. One hundred DNA samples from peripheral blood lymphocyte of healthy Japanese volunteers and one hundred Caucasian DNA samples (Caucasian Panel of 100 (HD100CAU); Coriell Institute for Medical Research, USA) were also used for the population study.

aCGH analysis

Genomic DNA was extracted from peripheral blood using the QIA quick DNA extraction kit (Qiagen, Hilden, Germany). Genomic copy number aberrations were analyzed using the Human Genome CGH Microarray 105A chip (Agilent Technologies, Santa Clara, CA) according to the method described elsewhere [19–22]. Briefly, 500 ng patient and reference DNA from healthy Japanese individuals were digested with restriction enzymes, Alu I and RsaI (Promega, Madison, WI). Cy-5 (patient) or Cy-3 dUTP (reference) were incorporated using Klenow fragment. The array was hybridized with labeled patient and reference DNA in the presence of Cot-1 DNA (Invitrogen, Carlsbad, CA) and blocking agents (Agilent Technologies) for 40 h at 65 °C, washed and scanned on the scanner (Agilent Technologies). Data was extracted using Agilent Feature Extraction software ver 9 with the default settings for aCGH analysis. Statistically significant aberrations were determined using the ADM-II algorithm in CGH Analytics software version 3.5 (Agilent Technologies). Breakpoints were defined as the start and stop location of the first and last probes, respectively, included in the algorithmically determined region of deletion.

Fluorescence in situ hybridization (FISH) analysis

Metaphase or prometaphase chromosomes were prepared from phytohemagglutinin-stimulated peripheral blood lymphocytes according to standard techniques. Four bacterial artificial chromosome (BAC) clones RP11-557O15 (14q13.1; 32,770,543//32,934,772), RP11-26M6 (14q13.2; 34,404,823//34,591,592), RP11-35M15 (14q13.2; 35,104,496//35,263,440) and RP11-81F13 (14q13.3; 36,297,744//36,467,869) that mapped around 14p13.2 were selected from the in-silico library build 2006 (UCSC Human genome browser, March 2006, http://genome.ucsc.edu/) and were purchased from Invitrogen (Germany). Clone RP11-112H5 (14q32.33; 105,798,044//105,952,495) was used for the marker of chromosome 14.

FISH analyses were performed using a combination of two BAC clones with the target clone and the marker clone [22]. Briefly, slide-mounted chromosomes were hardened at 65 °C for 150 min and then denatured in 70% formamide containing 2× standard saline citrate (SSC) at 70 °C for 2 min, and then dehydrated at −20 °C in ethanol. 1.5 μg of BAC clone DNA extracted using GenePrepStar PI-80X (Kurabo, Osaka, Japan) was labeled with SpectrumGreen TM-11-dUTP or SpectrumOrange TM-11-dUTP (Vysis, Downers Grove, IL) via nick translation and denatured at 70 °C for 5 min in the probe hybridization mixture including 50% of formamide, 2×SSC, and 10% dextran sulfate. Then, it was applied on the chromosomes, and incubated at 37 °C for 16 h. Slides were washed twice in 50% formamide containing 2×SSC at 43 °C for 15 min, 2×SSC for 5 min, 1×SSC for 5 min, 0.1% (v/v) Triton X-100/4×SSC for 5 min with shaking, 4×SSC for 5 min, then 2×SSC for 5 min and then mounted in antifade solution (Vector, Burlingame, CA) containing 4′,6-diamino-2-phenylindole (DAPI). Photomicroscopy was performed under a microscope equipped with a quad filter set containing single band excitation filters (Leica Microsystems, Tokyo, Japan).

Microsatellite marker analysis

Familial relationships and the origin of the 14q13.1q13.3 deletion for P1 were analyzed using the PRISM Linkage Mapping Set Panel 20 (Applied Biosystems Inc, Foster City, CA), which includes the primer sets of 14 microsatellite markers D14S261, D14S283, D14S275, D14S70, D14S288, D14S276, D14S63, D14S258, D14S74, D14S68, D14S280, D14S65, D14S985 and D14S292. PCR amplification using True Allele PCR Premix (Applied Biosystems Inc.) was performed according to the manufacture's protocol [23]. Then, the products were separated using the 3130xl Genetic Analyzer (Applied Biosystems Inc.) and analyzed by GeneMapper software (Applied Biosystems Inc.).

Mutation screening of the TULIP1 coding region

All 41 *TULIP1* exons from each patient were amplified by PCR using originally designed primers located on the both neighboring intronic sequences (Supplementary Table 2) according to the standard method. All amplicons were subjected to direct sequencing using the BigDye Terminator Cycle Sequencing kit (Applied Biosystems Inc.) according to the manufacturer's protocol. Sequencing reactions were separated using a 3130xl Genetic Analyzer (Applied Biosystems Inc.).

Because exon 33 was too large to analyze in the same manner with the other exons, it was divided into several parts. However, primers based on the exonic sequence could not be used for PCR due to the existence of the pseudogene of *TULIP1* which had quite similar sequences. When we use the primers on the coding region of exon 33 for PCR amplification, both the true *TULP1* and pseudo *TULIP1* were amplified. To circumvent this difficulty, the entire exon 33 was PCR amplified by both neighboring intron-based primers, which cannot amplify exon 33 of the pseudogene of *TULIP1*, and used as a template for direct sequencing using sequential exon-based primers.

Western blotting

Immortalized lymphocytes were collected by centrifugation at 1400×*g* and homogenized in sample buffer (50 mM Tris–HCl, pH 6.8, 2% sodium dodecyl sulfate (SDS), and 10% (v/v) glycerol) by sonication. β-Mercaptoethanol and bromophenol blue were added to cell lysates at final concentrations of 6% (v/v) and 0.003%, respectively. Proteins were resolved by SDS-PAGE and transferred to polyvinylidene difluoride membranes (Immobilon; Millipore, Billerica, MA). Membranes were blocked in phosphate buffered saline (PBS) containing 10% nonfat milk and 0.05% (w/v) Tween 20 for 1 h at room temperature. Membranes were then incubated with rabbit polyclonal anti-GARNL1 (TULIP1) (1:100 dilution, HPA00851; Atlas Antibodies, Sweden) or anti-β-actin monoclonal antibody (1:5000 dilution, A5441; Sigma, MO) overnight at 4 °C. Membranes were washed three times in PBS containing 0.05% Tween 20 and then incubated in HRP-conjugated secondary antibody for 1 h at 37 °C. Membranes were washed as before and signals were detected using SuperSignal West Pico Chemiluminescent Substrate (Thermo Fisher Scientific Inc., Rockford, IL) and FUJI RAS3000 (FUJI Film, Tokyo, Japan).

Zebrafish maintenance

Adult zebrafish (*Danio rerio*) were maintained at 28.5 °C under 14 h light/10 h dark cycle conditions. Embryos from natural crosses were collected a few minutes after spawning and cultured at 28.5 °C in water containing 0.006% NaCl and 0.00025% methylene blue. Embryos were staged according to morphology and hours post-fertilization (hpf) as described [4]. For *in situ* hybridization, *N*-phenylthiourea was added to culture water at a final concentration of 0.003% to avoid pigmentation of larvae.

Cloning of zebrafish tulip1

The sequence of the zebrafish tulip1 cDNA has been previously predicted using genomic data (GenBank accession XM_679242). In this study, the cDNA corresponding to the open reading frame (ORF) of *tulip1* was cloned by reverse transcription-polymerase chain reaction (RT-PCR) using primers designed based on the predicted sequence. Briefly, total RNA was extracted from 14 somite stage embryos using the RNeasy Mini Kit (Qiagen), and cDNA was synthesized using the Omniscript RT Kit (Qiagen) according to the manufacturer's instructions. All PCR amplification reactions were performed using KOD plus DNA polymerase (TOYOBO, Osaka, Japan). The 5′ and 3′ untranslated regions were also cloned by the rapid amplification of cDNA ends (RACE) method using the 5′-RACE Core Set (TAKARA, Otsu, Japan). (The sequences of the primers used in this study are shown in Supplementary Table 3.)

Whole mount in situ hybridization of tulip1 RNA

Whole-mount *in situ* hybridization was performed as described [4]. Briefly, digoxigenin-labeled antisense RNA probes, complementary to four partially overlapping regions of zebrafish *tulip1*, were synthesized. These probes corresponded to the following regions of *tulip1*; nt 511–1526, nt 1303–2337, nt 3714–4733 or nt 4527–5644 (relative the transcriptional start site GenBank accession AB476643 and AB476644). Because these four probes displayed identical staining patterns, they were used as a mixture. To enhance the contrast of the signal of *tulip1* in shield and bud stage embryos, specimens were soaked in transparency reagent (2:1 mixture of benzyl benzonate/benzyl alcohol).

Morpholino oligos and microinjection

Morpholino antisense oligos (MOs) were purchased from Gene Tools, LLC. The sequences of the two non-overlapping MOs used in this study were as follows: *tulip1* MO1, 5′-GAGATGTTTTGAAGAGCTAATGATA-3′; *tulip1* MO2, 5′-TCTTCCGTTAATTCCCTCAAACATG-3′. We also used the following control MO that does not match any zebrafish gene: 5′-AAACGTCTCTTGACTCTCCGCGATG-3′. MOs were dissolved in Danieau solution (5 mM HEPES, pH 7.6, 58 mM NaCl, 0.7 mM KCl, 0.4 mM $MgSO_4$, and 0.6 mM $Ca(NO_3)_2$) to a final concentration of at 10 μg/μl and stored at −20 °C. MOs were microinjected at 3 ng/nl as described [4].

Preparation of zebrafish head sections

Zebrafish embryos in appropriate stages were fixed in PBS containing 4% paraformaldehyde (PFA) at 4 °C overnight. The fixed embryos were gradually dehydrated with ethanol and then completely dehydrated using 2-propanol. Dehydrated embryos were soaked in xylene and embedded following transfer to Paraplast Plus embedding medium (McCormick Scientific, St. Louis, MO) under microscopic observation. Specimens were cut into serial sections (7 μm) and stained using Mayer's hematoxylin and eosin solutions.

Acknowledgment

This work was supported by the International Research and Educational Institute for Integrated Medical Sciences, Tokyo Women's Medical University, which is supported by the Program for Promoting the Establishment of Strategic Research Centers, Special Coordination Funds for Promoting Science and Technology, Ministry of Education, Culture, Sports, Science and Technology (Japan).

Appendix A. Supplementary data

Supplementary data associated with this article can be found, in the online version, at doi:10.1016/j.ygeno.2009.08.015.

References

[1] L.E. Vissers, J.A. Veltman, A.G. van Kessel, H.G. Brunner, Identification of disease genes by whole genome CGH arrays, Hum. Mol. Genet. 14 (Spec No. 2) (2005) R215–223.

[2] A.M. Slavotinek, Novel microdeletion syndromes detected by chromosome microarrays, Hum. Genet. 124 (2008) 1–17.

[3] T. Schwarzbraun, J.B. Vincent, A. Schumacher, D.H. Geschwind, J. Oliveira, C. Windpassinger, L. Ofner, M.K. Ledinegg, P.M. Kroisel, K. Wagner, E. Petek, Cloning, genomic structure, and expression profiles of TULIP1 (GARNL1), a brain-expressed candidate gene for 14q13-linked neurological phenotypes, and its murine homologue, Genomics 84 (2004) 577–586.

[4] M.A. Razzaque, T. Nishizawa, Y. Komoike, H. Yagi, M. Furutani, R. Amo, M. Kamisago, K. Momma, H. Katayama, M. Nakagawa, Y. Fujiwara, M. Matsushima, K. Mizuno, M. Tokuyama, H. Hirota, J. Muneuchi, T. Higashinakagawa, R. Matsuoka, Germline gain-of-function mutations in RAF1 cause Noonan syndrome, Nat. Genet. 39 (2007) 1013–1017.

[5] T. Hokama, M. Gushi Ken, N. Nosoko, Iron deficiency anaemia and child development, Asia Pac. J. Public Health 17 (2005) 19–21.

[6] M. Kodama, Y. Kai, S. Sugino, N. Inokuchi, T. Miike, Two siblings with interstitial deletion of chromosome 14 [46 XX, del (14) (q12 q13.3)], No To Hattatsu (in Japanese) 22 (1990) 61–65.

[7] S.K. Shapira, K.L. Anderson, A. Orr-Urtregar, W.J. Craigen, J.R. Lupski, L.G. Shaffer, De novo proximal interstitial deletions of 14q: cytogenetic and molecular investigations, Am. J. Med. Genet. 52 (1994) 44–50.

[8] P. Grammatico, S. de Sanctis, C. di Rosa, F. Cupilari, G. del Porto, First case of deletion 14q11.2q13: clinical phenotype, Ann. Genet. 37 (1994) 30–32.

[9] L. Govaerts, J. Toorman, M.V. Blij-Philipsen, D. Smeets, Another patient with a deletion 14q11.2q13, Ann. Genet. 39 (1996) 197–200.

[10] C.P. Chen, C.C. Lee, L.F. Chen, C.Y. Chuang, S.W. Jan, B.F. Chen, Prenatal diagnosis of de novo proximal interstitial deletion of 14q associated with cebocephaly, J. Med. Genet. 34 (1997) 777–778.

[11] G.P. Ramelli, L. Remonda, K.O. Lovblad, H. Hirsiger, H. Moser, Abnormal myelination in a patient with deletion 14q11.2q13.1, Pediatr. Neurol. 23 (2000) 170–172.

[12] E. Petek, B. Plecko-Startinig, C. Windpassinger, H. Egger, K. Wagner, P.M. Kroisel, Molecular characterisation of a 3.5 Mb interstitial 14q deletion in a child with several phenotypic anomalies, J. Med. Genet. 40 (2003) e47.

[13] P.H. Su, S.J. Chen, I.C. Lee, K.L. Wang, J.Y. Chen, H.M. Hung, C.F. Lee, Interstitial deletion of chromosome 14q in a Taiwanese infant with microcephaly, J. Formos Med. Assoc. 103 (2004) 385–387.

[14] D. Kamnasaran, C.P. Chen, K. Devriendt, L. Mehta, D.W. Cox, Defining a holoprosencephaly locus on human chromosome 14q13 and characterization of potential candidate genes, Genomics 85 (2005) 608–621.

[15] M. Kagami, Y. Sekita, G. Nishimura, M. Irie, F. Kato, M. Okada, S. Yamamori, H. Kishimoto, M. Nakayama, Y. Tanaka, K. Matsuoka, T. Takahashi, M. Noguchi, Y. Tanaka, K. Masumoto, T. Utsunomiya, H. Kouzan, Y. Komatsu, H. Ohashi, K. Kurosawa, K. Kosaki, A.C. Ferguson-Smith, F. Ishino, T. Ogata, Deletions and epimutations affecting the human 14q32.2 imprinted region in individuals with paternal and maternal upd(14)-like phenotypes, Nat. Genet. 40 (2008) 237–242.

[16] T. Ogata, M. Kagami, A.C. Ferguson-Smith, Molecular mechanisms regulating phenotypic outcome in paternal and maternal uniparental disomy for chromosome 14, Epigenetics 3 (2008) 181–187.

[17] S. Saitoh, T. Wada, Parent-of-origin specific histone acetylation and reactivation of a key imprinted gene locus in Prader-Willi syndrome, Am. J. Hum. Genet. 66 (2000) 1958–1962.

[18] K. Takano, E. Nakagawa, K. Inoue, F. Kamada, S. Kure, Y. Goto, A loss-of-function mutation in the FTSJ1 gene causes nonsyndromic X-linked mental retardation in a Japanese family, Am. J. Med. Genet. B Neuropsychiatr. Genet. 147B (2008) 479–484.

[19] M.T. Barrett, A. Scheffer, A. Ben-Dor, N. Sampas, D. Lipson, R. Kincaid, P. Tsang, B. Curry, K. Baird, P.S. Meltzer, Z. Yakhini, L. Bruhn, S. Laderman, Comparative genomic hybridization using oligonucleotide microarrays and total genomic DNA, Proc. Natl. Acad. Sci. U. S. A. 101 (2004) 17765–17770.

[20] A. Bartocci, P. Striano, M.M. Mancardi, M. Fichera, L. Castiglia, O. Galesi, R. Michelucci, M. Elia, Partial monosomy Xq(Xq23→qter) and trisomy 4p (4p15.33→pter) in a woman with intractable focal epilepsy, borderline intellectual functioning, and dysmorphic features, Brain Dev. 30 (2008) 425–429.

[21] G.A. Toruner, D.L. Streck, M.N. Schwalb, J.J. Dermody, An oligonucleotide based array-CGH system for detection of genome wide copy number changes including subtelomeric regions for genetic evaluation of mental retardation, Am. J. Med. Genet. A 143A (2007) 824–829.

[22] K. Shimojima, M. Adachi, M. Tanaka, Y. Tanaka, K. Kurosawa, T. Yamamoto, Clinical features of microdeletion 9q22.3 (pat), Clin. Genet. 75 (2009) 384–393.

[23] K. Shimojima, K. Tanaka, T. Yamamoto, A de novo intra-chromosomal tandem duplication at 22q13.1q13.31 including the Rubinstein-Taybi region but with no bipolar disorder, Am. J. Med. Genet. A 149A (2009) 1359–1363.

Index for Supplemental Materials to K. Shimojima et al. "*TULIP1* haploinsufficiency with brain development delay"

Supplemental Fig. 1: Clinical evaluation for P1 with a 14q13.1q13.3 deletion. (A) Electroencephalography indicating high voltage θ bursts during convulsions. T1-(C) and T2-(D) weighted brain MRIs at the age of 3 years indicating diffuse mild brain atrophy.

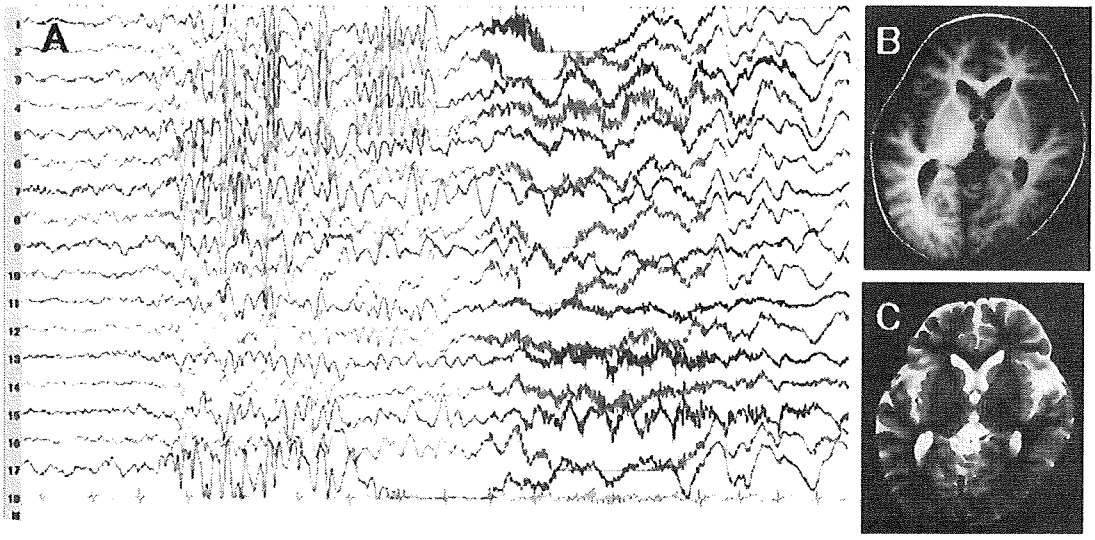

Supplemental Fig. 2: Sequence analysis of *TULIP1* indicating single missense mutations in four individuals. The portion of each TULIP1 sequence containing the missense mutation is shown with the predicted amino acid sequence at the top. Proband identification numbers are indicated at left (boxes).

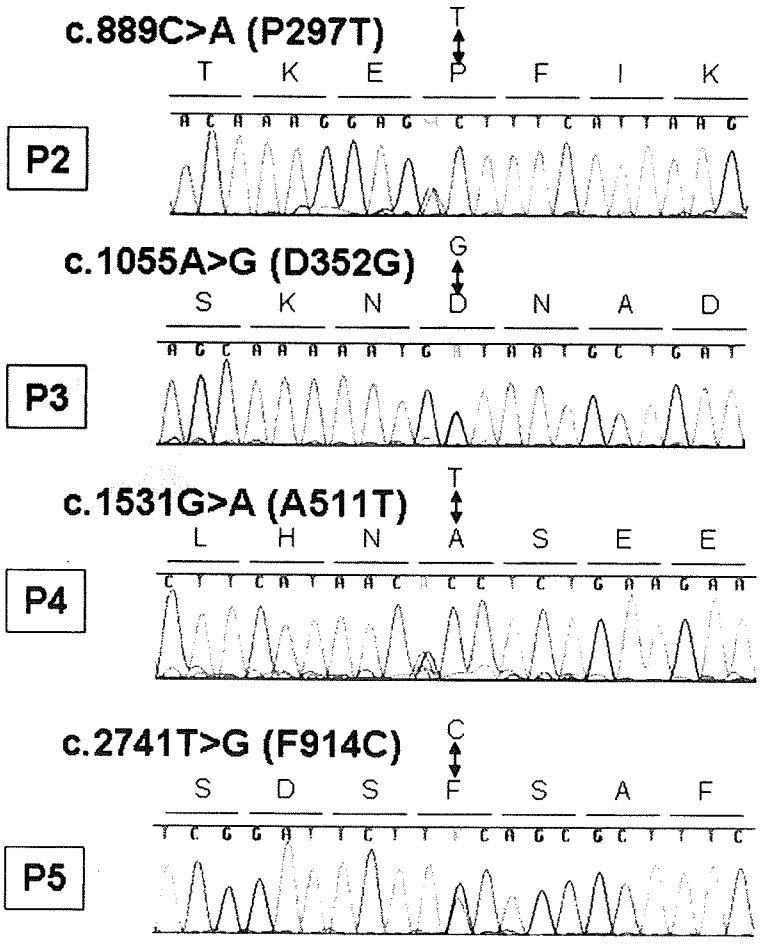

Supplemental Fig. 3: Family trees of the patients with deletions or mutations of *TULIP1*. Squares represent males and circles represent females. Filled squares and circles indicate the patients with developmental delay. m: *TULIP1* mutation.

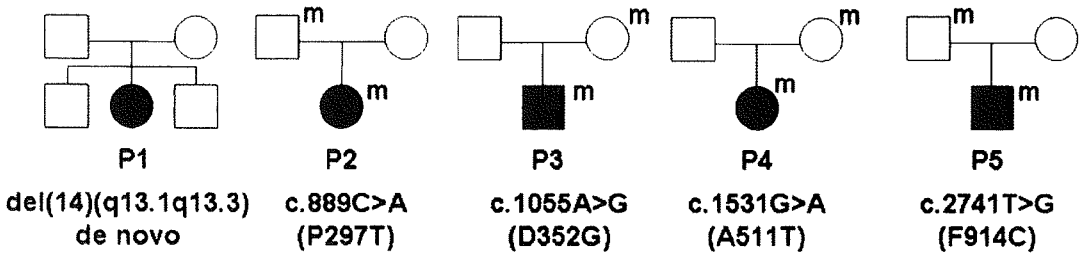

Supplemental Fig. 4: Comparison of mammalian TULIP1 amino acid sequences. Regions of the amino acid sequence containing the single *TULIP1* missense mutations identified in four mentally retarded patients are shown. Arrows indicate the position of the missense mutations. P297 and F914 are conserved among species, but D352 and A511 are not.

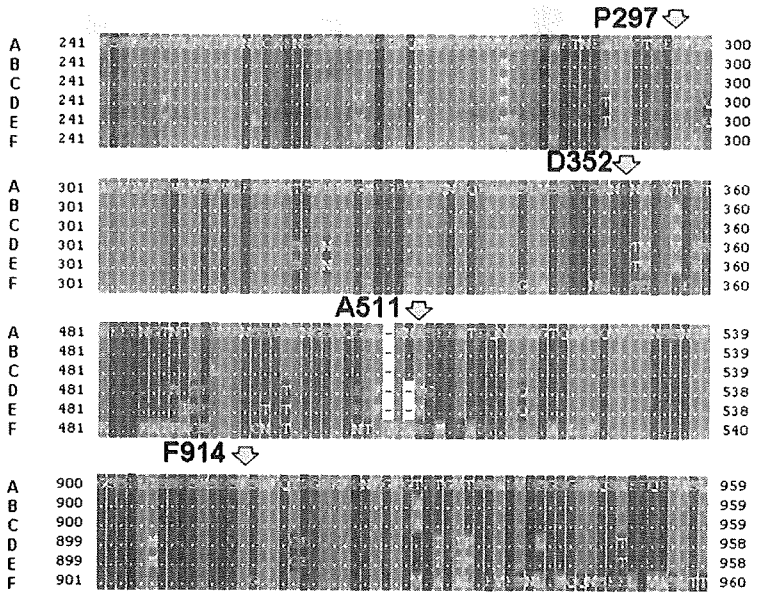

A: Homo sapiens NP_055805
B: Pan troglodytes (chimpanzee) XP_001140817
C: Macaca mulatta (rhesus monkey) XP_001088522
D: Mus musculus (house mouse) NP_001106185
E: Rattus norvegicus (Norway rat) XP_001079197
F: Monodelphis domestica (gray short-tailed opossum) XP_001363188

Mitochondrion 10 (2010) 32–37

Contents lists available at ScienceDirect

Mitochondrion

journal homepage: www.elsevier.com/locate/mito

Mitochondrial DNA variants in a Japanese population of patients with Alzheimer's disease

Noriko Tanaka [a,b,*], Yu-ichi Goto [b], Jun Akanuma [b], Mayuko Kato [b], Toru Kinoshita [b], Fumio Yamashita [b], Masashi Tanaka [c], Takashi Asada [d]

[a] Department of Biostatistics, Harvard School of Public Health, 655 Huntington Avenue, Boston, MA 02115, USA
[b] Department of Mental Retardation and Birth Defect Research, National Institute of Neuroscience, National Center of Neurology and Psychiatry, 4-1-1, Ogawahigashi-machi, Kodaira-shi, Tokyo 187-8502, Japan
[c] Department of Genomics for Longevity and Health, Tokyo Metropolitan Institute of Gerontology, 35-2 Sakae-cho, Itabashi-ku, Tokyo 173-0015, Japan
[d] Department of Neuropsychiatry, Institute of Clinical Medicine, University of Tsukuba, Tsukuba, 1-1-1, Tennodai, Tsukuba-shi, Ibaraki 305-8571, Japan

ARTICLE INFO

Article history:
Received 11 January 2009
Received in revised form 10 August 2009
Accepted 18 August 2009
Available online 22 August 2009

Keywords:
mtDNA
Alzheimer disease
Rare variant
Association study
APOE
Sequencing

ABSTRACT

The evidence for the role of mitochondria in Alzheimer's disease (AD) has been well investigated, based on the amyloid hypothesis and its relation to the mitochondrial dysfunction due to oxidative stress. However, contrasting reports describe an unclear picture on the relationship between AD and mitochondrial DNA (mtDNA) variations. Therefore, we analyzed complete mtDNA sequences from 153 AD patients and 129 normal control subjects to determine if inherited mtDNA polymorphisms or rare variants, or both contribute to the etiology of late-onset AD. The results reported herein indicate that inherited mtDNA common polymorphisms could not be the single major causes of AD but that some rare variants in the protein-coding-region may have protective effects for high-risk populations with the APOE e4 allele. Furthermore, our results support the idea that the np956–965 poly-c insertion and 856A>G variant might be a riskfactor for AD.

1. Introduction

Alzheimer's disease [AD (MIM 104300)] is the most common neurodegenerative disorder, characterized clinically by progressive cognitive decline, and pathologically by the presence of senile plaques composed primarily of amyloid-β peptide (Aβ) and neurofibrillary tangles made up mainly of hyperphosphorylated tau protein. Almost all cases are sporadic and non-familial, with a complex etiology that is intertwined with genetic and environmental risk factors. Decades of research have provided evidence for only a single gene, apolipoprotein E (APOE), as the major genetic risk factor for sporadic AD.

There is evidence of a role for mitochondria in AD based on the amyloid hypothesis and for a relationship between AD and mitochondrial dysfunction due to oxidative stress (Pereira et al., 2005; Cacabelos et al., 2005; Chen et al., 2006; Crouch et al., 2007; Grazina et al., 2006). Moreover, many observations suggest that mitochondrial genetic abnormalities contribute to the pathogenic amyloid metabolism in sporadic AD and that Aβ oversecretion stimulated by mitochondrial dysfunction would serve a critical role in the pathogenesis of the disease (Nunomura et al., 2001; Pratico et al., 2001; Reddy et al., 2004; Beal, 2004; Khan et al., 2000).

The putative role of mtDNA polymorphisms in AD pathogenesis is supported by higher incidence of AD in the mothers of the probands, which has been connected with the maternal inheritance of mtDNA (Beal, 1998; Bonilla et al., 1999). Mitochondrial SNPs (mtSNPs) and/or their clusters (haplogroups) are thought to affect susceptibility to AD by influencing mitochondrial metabolism (Chagnon et al., 1999; Carrieri et al., 2001). Therefore genetic epidemiological studies have been used to ascertain the presence of pathogenic rare variants or polymorphisms of mtDNA. In addition to the report of a relationship between oxidative phosphorylation (OXPHOS) performance and mitochondrial haplogroups (Ruiz-Pesini et al., 2000), more genetic epidemiological studies on mtDNA of mostly Caucasian populations have reported associations between mtDNA common polymorphisms or mtDNA haplogroups and AD (Chagnon et al., 1999; Carrieri et al., 2001; Mancuso et al., 2007; Fesahat et al., 2007; Maruszak et al., in press; van der Walt et al., 2004). However, these associations still remain unclear (Grazina et al., 2006; Howell et al., 2005), because haplogroups are defined by using common polymorphisms in each ethnic group (Torroni et al., 1996). The distribution of mtDNA allele

* Corresponding author. Address: Department of Biostatistics, Harvard School of Public Health, 655 Huntington Avenue, Boston, MA 02115, USA. Tel.: +1 617 432 2416; fax: +1 617 432 5619.
E-mail address: nyamaguc@hsph.harvard.edu (N. Tanaka).

1567-7249/$ - see front matter © 2009 Elsevier B.V. and Mitochondria Research Society. All rights reserved.
doi:10.1016/j.mito.2009.08.008

frequency varies considerably with the population studied, which implies that haplogroup analysis is insufficient across populations.

Identifying AD-specific mtDNA mutations has been more of a challenge. At present, eight different mtDNA point mutations or variations have been reported either in only AD patients or at higher frequencies in AD patients than in control subjects (Grazina et al., 2006). However, as well as the haplogroups analysis, the contribution of inherited mitochondrial rare variants to the pathogenesis of AD is also unclear, because most of the association studies have not been replicated in other populations.

Additionally, there are only a few research studies that have explored the association between AD and the non-coding control region (CR), although variants localized in this region have been reported to be related with aging (Edris et al., 1994; Wang et al., 1997; Coskun et al., 2003, 2004).

As the impact of mtDNA polymorphisms or rare variants on AD etiology remains controversial, we analyzed the complete mtDNA sequences of Japanese AD patients and their age-matched Japanese control subjects to determine the contribution of inherited mtDNA variations, polymorphisms or rare variants, to the etiology of late-onset AD.

2. Subjects and methods

2.1. Subjects

This case-control association study was approved by the Institutional Review Board of the National Center of Neurology and Psychiatry (NCNP). Cases included outpatients who attended the Memory Clinic of Musashi Hospital, NCNP (Asada et al., 2000). The diagnosis of probable AD based on the NINCDS-ADRDA criteria was made after detailed examination, including neuroimaging (magnetic resonance imaging and single photon emission computed tomography) and a series of neuropsychological batteries. Cognitively intact spouses of patients were asked to take part in our prospective cohort study of AD as the control subjects, who were selected and matched based on sex and age (within a range of 3 years). Information about both the AD patients and control subjects was obtained by interviews of relatives, exclusively living spouses or first-degree relatives, and when possible, multiple relatives were interviewed to improve the accuracy of the data. To analyze complete mtDNA sequences, we randomly selected 200 AD patients and 200 control subjects among 758 AD (267 men and 491 women) patients and 557 control (240 men and 317 women) subjects, respectively. To explore sporadic late-onset AD objectively, we excluded from statistical analysis those subjects whose age at onset was less than 65 years. The backgrounds of the final subjects, including 153 AD patients and 129 control subjects, are shown in Table 1. In all of the subjects, the observed APOE genotypes fitted with the expected Hardy–Weinberg equilibrium (HWE) results ($p = 0.96$, AD; $p = 0.98$, control).

To categorize the variants into polymorphisms and rare variants, we used additional data: the data for a young male group from the mtSNP database ($N = 96$) and the controls who had been excluded from the analysis (i.e. $N = 71$, controls under 65 years old). The total sample size for estimation of allele frequency was 296.

Table 1
Background of the subjects.

	Control ($n = 129$)	Patients with AD ($n = 153$)	p-Value
Age, mean ± SD	72.6 ± 5.6	76.8 ± 5.6	<0.0001
Sex, No (%) female	75 (58.1)	100 (65.4)	0.213
APOE e4 carriers	32 (25.6)	69 (45.4)	0.0007
Smoking status, No (%) yes	48 (38.7)	52 (34.9)	0.515
Drinking status, No (%) yes	40 (32.0)	36 (24.2)	0.149
Education (years)	10.7 ± 2.6	10.1 ± 2.8	0.060

2.2. Direct sequencing of total mtDNA

DNA extraction, PCR and total mtDNA sequencing were done as described previously (Akanuma et al., 2000). To minimize the adverse effect of the nuclear pseudogene, we employed the long PCR method to prepare the sequencing reaction template. After two overlapping segments, such as S1 and L1, were amplified, three overlapping fragments designed S2 (derived from S1), L2A and L2B (from L1) were amplified by the AccuTaq LA Polymerase (Sigma). We used the following oligonucleotide pairs for amplification: S1, 5′-GAATCGGAGGACAACCAGTA-3′/5′-GCGGGAGAAGTA GATTGAAG-3′, L1, 5′-CTTAATTCCATCCACCCTCCTCTCCCTAGG-3′/ 5′-CTTGTGCGGGATATTGATTTCACGGAGGATGG-3′, S2, 5′-TCGGAG GACAACCAGTAAGC-3′/5′-GATTGAAGCCAGTTGATTAGGG-3′, L2A, 5′-CCTAGGAGGCCTGCCCCCGC-3′/5′-GGGTTAACGAGGGTGGTAAGG ATGGG-3′ and L2B, 5′-ACCACAACACAATGGGGCTCACTCA-3′/5′-CG GAGGATGGTGGTCAAGGG-3′. PCR parameters included: 96 °C at 10 s followed by 40 cycles of 94 °C for 15 s, 50 °C for 5 s, and 60 °C for 4 min in the GeneAmp PCR System 2400 (PE Applied Biosystems). PCR products were purified directly using Microspin S-400 HR Columns (Amersham Pharmacia Biotech). With 96 primer sets designed for sequencing (35 primers for S1, 39 for L2A, 22 for L2B), we sequenced S2, L2A and L2B fragments using the BigDye Terminator Cycle Sequencing Ready Reaction kit (PE Applied Biosystems). Unincorporated dye terminators were removed by the MultiScreen 96-Well Filtration Plate (Millipore) and the reaction product was analyzed by using an ABI 3700 automated sequencer according to the manufacturer's protocols.

2.3. Statistical analysis

The statistical significances of the differences between the AD and control groups were determined with the chi-square (χ^2) test for categorical variables, and with the t-test for continuous variables. The HWE was tested by using the chi-square goodness-of-fit test. The one-sample binomial exact test was used to determine the thresholds of grouping the variants. Multiple logistic regression analyses were performed to assess the associations of individual minor polymorphisms or rare variants with the risk of AD, with adjustment for the conventional risk factors, age, sex, educational background, smoking status, alcohol consumption and APOE e4 allele status. The difference in mean number of variations, rare variants, and Grantham's value between the AD and control groups was examined by performing the Wilcoxson rank sum test. The significance level for pair-wise comparison was set to 0.05. Study-wide significance (P_{study}) was empirically evaluated by permutation testing.

Assuming approximately 100 independent tests were performed in this study, this sample has more than 50% power to reject the null hypothesis of no association of mtDNA variants with AD at $p < 0.05$ for 10% risk alleles with a 2.0 GRR, and more than 70% power for more than 20% risk alleles.

3. Results

3.1. Definition of mtDNA polymorphisms and rare variants

Sequence analysis of the entire mitochondrial genomes from 153 AD patients and 129 control subjects revealed a total of 962 variations. The distribution of variations among the protein-coding-region included single nucleotide variations as well as insertions, deletions, and substitutions in the hypervariable regions.

Out of the total variations, 840 (76%) variations have already been reported and listed in the MITOMAP, a human mitochondrial genome database, or in the mtSNP database, a human mitochondrial polymorphism database. Among those variations, we defined as "rare variants" those with a minor allele frequency (MAF) of less than 2% in control groups ($N = 296$; 200 control subjects + 96 young males). We set the threshold at 2% because the left-sided p-value computed for the allele with more than 2% frequency was less than 0.05, which provides sufficient evidence to reject the null hypothesis that the minor allele frequency in the population was less than 1%. All other variations were defined as "polymorphisms". Eventually, we determined 711 rare variants and 251 polymorphisms from our definitions.

3.2. Association of minor alleles of variants with AD

We presented 41 common polymorphisms of which the frequency was more than 10% in the AD or control group and 17 variants that were previously reported (Supplementary Table 1). Among the 41 polymorphisms observed, only the minor allele of 303_304insC polymorphism was found to be significantly, but weakly associated with AD ($p = 0.03$). However, these results were far from significant after permutation testing ($P_{study} = 0.60$). No polymorphism had interaction effects with the APOE e4 allele status.

Among these 58 variants, only two variants in the 12S rRNA region, the np956–965 insertion and 856A>G transition, were confirmed to have positive reproducible results. All other variants either were not observed in our subjects or confirmed negative association. Moreover, these two rare variants were the only observable mutations in the AD group and were previously reported by Shoffner et al. (1993) and Tanno et al. (1998), though the number of inserted base-pairs at the 956 position vary slightly: 5 bp in Shoffer's sample, 3 bp in Tannno's sample, and 3 bp and 4 bp in our sample.

3.3. Association of the number of variants per person with AD

There was no statistically significant difference between AD and control group for the number of variants or for that of rare variants in the entire mtDNA ($p = 0.37$, 0.38). Analyzing each region separately, we observed a few statistically significant differences between AD cases and the controls. In the region of the entire rRNA and ATP8 genes, the number of variants was significantly larger in the AD group than in the controls ($p = 0.03$, 0.02). On the contrary, the controls had more variants on average in the CO_2 region than AD ($p = 0.02$). Limiting the analysis to the rare variants, we observed a statistically significant result only in the D-loop region ($p = 0.028$, Table 2).

3.4. Examination of the interaction effect of APOE and mtDNA rare variants

For the entire coding-region, there were no significant differences in the mean of the number of rare variants between the AD and the control groups. However, a possible interaction was observed between the APOE e4 allele and the number of rare variants to enhance AD risk ($p = 0.035$). For the individuals with the e4 allele, the average number of rare variants in the coding-region in the control group, 3.09, was significantly higher than that in the AD group, 1.94 ($p = 0.036$). For the e4 non-carriers, the average number of rare variants for the AD patients was not different from that in the control group. To explore how the rare variants modify the AD risk in APOE e4 carriers, we calculated the odds ratios (ORs) at the various cut-off points of the number of rare variants (Fig. 1). The results suggested that the OR declined with more rare variants and that APOE e4 had no effect in the group having more than two rare variants (OR = 1.50, $p = 0.39$). In the subjects with 1 rare variants or none, OR was estimated to be 3.96 ($p = 0.005$). Thus, only the e4 carriers in the control group had one more rare variant than the AD group on average: and by limiting the analysis to non-synonymous rare variants only, this tendency was the same.

Additionally, we explored which rare variant contributed to this difference of the non-synonymous rare variants in the coding-region. The results from the analysis of each gene showed that there were interaction effects with the APOE e4 allele in only two regions, ND2 (OR = 3.50, $p < 0.0001$ without rare variants group; OR = 0.79, $p = 0.84$ with rare variants group) and ND5 (OR = 3.12, $p = 0.0002$ without rare variants group; OR = 1.11, $p = 0.88$ with rare variants group).

Table 2
Distribution of the number of rare variant.

Region		No. of variants observed in (control/case)	Control				Case				
			Mean	Median	SE	Range	Mean	Median	SE	Range	p-Value
All region		455/470	4.19	3	3.2	0–13	4.1	3	3.32	0–17	0.375
D-loop		70/68	0.85†	1	1.04	0–5	1.03†	1	1.29	0–6	0.028
rRNA	12SrRNA	16/21	0.16	0	0.48	0–3	0.26	0	0.63	0–3	0.135
	16SrRNA	16/17	0.19	0	0.41	0–2	0.18	0	0.42	0–2	1
	All rRNA	32/38	0.34	0	0.66	0–4	0.44	0	0.76	0–3	0.29
tRNA	All tRNA	23/39	0.24	0	0.48	0–2	0.25	0	0.47	0–2	0.83
Coding-region	All genes		2.5 (0.92)	2 (1)	2.15 (1.07)	0–10 (0–4)	2.3 (0.71)	2 (1)	2.08 (0.94)	0–13 (0–5)	0.58 (0.58)
	ND1	22/26	0.21 (0.06)	0 (0)	0.48 (0.24)	0–2 (0–1)	0.23 (0.09)	0 (0)	0.53 (0.29)	0–3 (0–1)	0.19 (0.07)
	ND2	32/23	0.34 (0.14)	0 (0)	0.61 (0.35)	0–2 (0–1)	0.23 (0.08)	0 (0)	0.53 (0.29)	0–3 (0–2)	0.24 (0.26)
	CO1	35/33	0.32 (0.05)	0 (0)	0.57 (0.23)	0–2 (0–1)	0.25 (0.06)	0 (0)	0.53 (0.24)	0–2 (0–1)	0.65 (0.29)
	CO2	17/14	0.19 (0.06)	0 (0)	0.43 (0.24)	0–2 (0–1)	0.11 (0.02)	0 (0)	0.33 (0.14)	0–2 (0–1)	0.10 (0.51)
	ATP8	4/7	0.05 (0.03)	0 (0)	0.23 (0.17)	0–1 (0–1)	0.08 (0.03)	0 (0)	0.31 (0.20)	0–2 (0–2)	0.96 (0.42)
	ATP6	20/20	0.17 (0.11)	0 (0)	0.45 (0.40)	0–3 (0–3)	0.14 (0.04)	0 (0)	0.37 (0.19)	0–2 (0–1)	0.66 (0.58)
	CO3	22/13	0.03 (0.06)	0 (0)	0.17 (0.27)	0–1 (0–1)	0.01 (0.01)	0 (0)	0.11 (0.11)	0–1 (0–1)	0.18 (0.23)
	ND3	3/7	0.02 ()	0 ()	0.15 ()	0–1 ()	0.05 ()	0 ()	0.21 ()	0–1 ()	0.48 ()
	ND4L	4/10	0.05 (0)	0 (0)	0.29 (0)	0–2 (0–0)	0.07 (0.01)	0 (0)	0.3 (0.11)	0–2 (0–1)	0.34 (0.26)
	ND4	25/26	0.27 (0.07)	0 (0)	0.53 (0.27)	0–3 (0–1)	0.25 (0.03)	0 (0)	0.48 (0.18)	0–2 (0–1)	0.25 (0.18)
	ND5	48/41	0.41 (0.17)	0 (0)	0.67 (0.45)	0–3 (0–3)	0.40 (0.18)	0 (0)	0.62 (0.38)	0–3 (0–1)	0.83 (0.78)
	ND6	14/17	0.16 (0.05)	0 (0)	0.39 (0.23)	0–2 (0–1)	0.14 (0.05)	0 (0)	0.39 (0.22)	0–2 (0–1)	0.34 (0.26)
	cytb	33/32	0.30 (0.10)	0 (0)	0.58 (0.30)	0–3 (0–1)	0.27 (0.11)	0 (0)	0.50 (0.31)	0–2 (0–1)	0.97 (0.76)

For coding-region, the distribution and p-value of the number of non-synonymous variations per person is shown in the parenthesis.

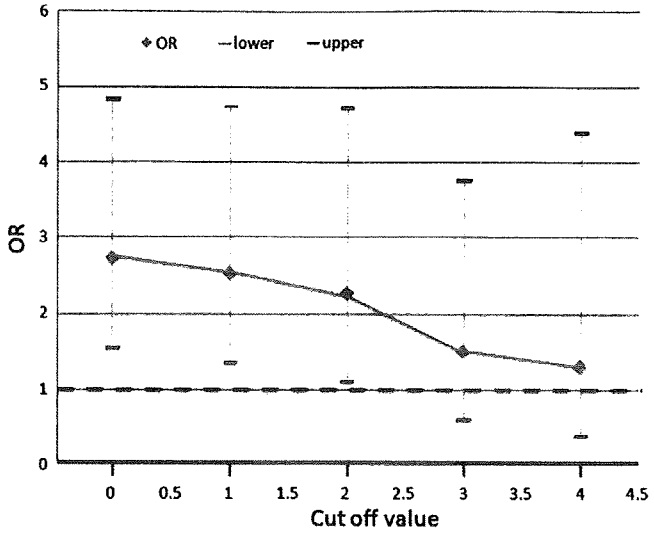

Fig. 1. Estimated odds ratios shifting the cut-off values of the number of rare variants per person. Odds ratios were estimated from the multivariate logistic regression model, adjusted with age, sex, smoking status, drinking history and educational backgrounds. At each cut-off value, *x*, the odds ratio was estimated from the observations that have *x* or more rare variants in the mtDNA coding-region.

4. Discussion

Even with ample evidence implicating a role of mitochondria in the pathogenesis of AD, a conclusive association of mtDNA variants with AD has yet to be made. So, we explored whether each mtDNA variant was associated with AD in Japanese subjects. The results show that (1) inherited mtDNA common polymorphisms cannot be the single major cause of AD, (2) the np956–965 poly-c insertion and 856A>G variant may increase the risk for AD, and (3) some rare variants in the protein-coding-region may have protective effects in patients with the APOE e4 allele.

4.1. 303_304insC polymorphism, mtDNA rare variants in 12S rna and AD

Among the identified 251 polymorphisms, none were reproducibly associated with AD. In our study, 303_304insC in CR was weakly associated with AD at nominal levels. This length polymorphism has been recently identified as a frequent hotspot of rare variants in human neoplasia (Parrella et al., 2003) and reported not to be a causative risk factor but an early event in colorectal (Legras et al., 2008) and gallbladder (Tang et al., 2004) adenomas. However, we are the first to report an association between this 303_304insC and the risk of AD. This poly-C insertion is known as polycytosine with a thymine interruption, which has been recently reported to generate quantitative and qualitative differences in prematurely terminated transcripts (Asari et al., 2007). Hence, the 303_304insC polymorphism might have changed the OXPHOS efficiency. Further studies are needed to replicate the association and to confirm the functional effects of this 303_304insC polymorphism on AD etiology.

The only rare variant observed in only AD patients was reportedly the np956–965 insertion found among the European (Shoffner et al., 1993) and Japanese populations (Tanno et al., 1998). The insertion of cytosines would expand the size of a proposed loop structure of the central region in the 12S rRNA and might alter its function (Zwieb et al., 1981). This insertion occurs at the boundary of helix22 and helix20 in *Escherichia coli* (*E. coli*) 16S RNA, and consists of the platform of the structure of the 30S ribosomal subunit (Wimberly et al., 2000). Compared to the region of the other mammalian mitoribosome, this region is not highly conserved, which suggests that its function would not be very important for sustaining life. The mitoribosomal protein S8 combines with this region in *E. coli*, whereas the human mitochondrial homologue of S8 has not yet been identified (Suzuki et al., 2001), suggesting that there might be a binding site of a protein that is specific to mitochondria in the region surrounding 956–965 in human mitochondrial 12S rRNA. In that case, the cytosine base insertion would affect binding activity. Alternatively, since the ribosomal subunit has an important role in the decoding process, it has been suggested that variations in 12S rRNA result in translational misreading and mitochondrial dysfunction. Although the frequency of the insertion at 956–965 is very low in both populations, our results suggest that this insertion could be one of the genetic risk factors for AD.

For validating our findings of an association between AD and 1 cytosine insertion at 303 in D-loop, 856A>G variant and 956–961 insertion variations in 12S rRNA, we extracted and compared frequency data from the mtSNP database and mitochondrial disease controls (Table 3). Using all Japanese AD cases and controls data, we estimated the crude odds ratio for 303–304insC to be 1.7 ($p = 0.01$), which was almost equal to that estimated from our case-control study data only. More than three cytosine insertion variations at 956–965 were observed in the Japanese young male group (1/96), Japanese Parkinson's disease [MIM168600] group (1/96), Japanese non-insulin-dependent diabetes mellitus (NIDDM) [MIM121853] group (6/192) and the group of Saami and Berbers (Achilli et al., 2005) (2/39), as well as in the AD group (6/250). The frequency of insertion variants with more than three cytosines was high in the NIDDM group. Also, the 856A>G variant was observed in the NIDDM group and the obese young male group. It is now widely recognized that NIDDM and AD share several common abnormalities including impaired glucose metabolism, increased oxidative stress, insulin resistance and amyloidogenesis (de la Monte and Wands, 2005; Hoyer, 1998, 2002; Zhao and Townsend, 2009; Cole and Frautschy, 2007). Our findings suggest that these rare variants in the 12S rRNA are related to the activity of OXPHOS that leads to a common pathological condition in AD and NIDDM.

4.2. The number of mtDNA rare variants, APOE, and AD

Our results showed that the genes from the control group had more replacement substitutions than those in the AD group, where areas mtDNA from the AD group had a higher frequency of rare variants in the non-coding-regions than the control group. The results are in agreement with those of Elson et al. (2006), whose analysis of the entire mtDNA coding-region of Caucasian AD patients against a control group showed no evidence for an etiological role of haplogroup-associated polymorphisms. Although our results were reproducible, it is not clear why more rare variants were observed in protein-coding-region in the control group than in the AD one.

Our result suggested that the rare variants in ND2 gene was the most susceptible to AD, furthermore, these variants modified the effect of APOE e4 allele status on the development of AD. Although the APOE e4 allele is strongly linked to AD pathology, its mode of action is unknown; though several mechanisms have been proposed (Buttini et al., 1999; Holtzman et al., 2000; Ji et al., 2002; Nathan et al., 1994; Tesseur et al., 2000; Raber et al., 2000). Through interactions with the Aβ peptide, APOE e4 polymorphism may increase Aβ deposition in plaques and impair its clearance. However, APOE may act through other pathways that may or may not involve Aβ. Some recent hypotheses on the contribution of the APOE e4 to the pathogenesis of AD suggest that fragments

Table 3
Frequency of rare variants that observed in AD group and neither in the control group nor young Japanese men reported with mtSNP database.

	Locus variation												
	N	303–315				956–964							856
		del	ins c	ins cc	ins ccc	del	ins c	$t \rightarrow$ ccccc	$t \rightarrow$ cccc	$t \rightarrow$ ccc	$t \rightarrow$ cc	$t \rightarrow$ c	$a \rightarrow$ g
Japanese													
Patients with AD	154	1	82	13	2	0	0	1	1	0	1	0	1
AD in mtSNP	96	0	43	27	0	0	1	0	3	1	0	0	2
All Japanese AD group	250	1	125	40	2	0	1	1	4	1	1	0	3
%	100	0.4	50.0	16.0	0.8	0.0	0.4	0.4	1.6	0.4	0.4	0.0	1.2
AD controls	200	2	89	26	0	0	2	0	0	0	0	0	1
Young male	96	0	37	21	0	0	2	0	0	1	0	0	0
All Japanese control group	296	2	126	47	0	0	4	0	0	1	0	0	0
%	100	1.4	42.6	15.9	0	0	1.4	0	0	0.7	0	0	0
Patients with PD	96	3	42	15	0	0	0	0	0	1	0	2	0
Centenarian	96	3	44	22	1	0	2	0	0	0	0	1	1
Patients with NIDDM	192	1	81	40	1	0	3	1	1	4	5	1	1
Obese young male	96	2	44	10	1	0	1	0	1	0	0	0	4
mtSNP													
Ingman (Nature 408: 708, 2000)	86	0	34	7	0	0	0	0	0	0	0	0	0
Finnila (Am J Hum Genet 68: 1475, 2001)	192	2	104	18	0	0	0	0	0	0	0	0	0
Herrnstadt (Am J Hum Genet 70: 1152, 2002)	560	–	–	–	–	2	2	0	0	0	0	0	0
Kong (Am J Hum Genet 73: 671, 2003)	48	1	20	11	0	0	1	0	0	0	0	0	0
Palanichamy (Am J Hum Genet 75: 966, 2004)	75	0	27	10	0	0	0	0	0	0	0	0	0
Achilli (Am J Hum Genet 75: 190, 2004)	62	0	25	12	0	0	0	0	0	0	0	0	0
Thangaraj (Science 308: 996, 2005)	15	0	0	0	0	0	0	0	0	0	0	0	0
Achilli, Rengo, et al. (Am J Hum Genet 76: 883, 2005)	39	0	14	0	0	1	0	0	2	0	0	0	0
All reference group	1557	12	435	145	3	3	9	1	4	5	5	4	0
%	100	0.8	27.9	9.3	0.2	0.2	0.6	0.06	0.3	0.3	0.3	0.3	0

of processed APOE can disrupt mitochondrial regulation of energy and glucose metabolism in neurons (Mahley et al., 2006). It is reported that the APOE4 genotype could modulate the effect of mtDNA haplogroups (Carrieri et al., 2001; Maruszak et al., in press). However, we did not observe an interaction effect of APOE with any common polymorphisms. We speculate that the distribution of rare variants might be related to haplogroups. Thus some inherited combination of multiple rare variants may cause some specific expression that defects the harmful effects of APOE e4. In this regard, further study on various ethnic populations and expression analysis might be needed.

4.3. Study limitations

The sample size of our study was not large enough for detecting 0.5% or much less rare variants, so we would likely miss pathogenic mutations. However, there is a high possibility that most rare variants in the Japanese population were detected in our samples, because we identified more variants than previously reported in the mtSNP database.

This study did not address the role of mtDNA heteroplasmy in AD. Acquired somatic mtDNA rare variants in tissues of relevance to AD would not have been detected in the blood samples, yet blood DNA typically exhibits much less heteroplasmy than non-dividing tissues (Jazin et al., 1996). In the 284 DNA samples tested, three (1.1%) samples had one or more 'heteroplasmic' calls. Although the significance of these heteroplasmic mutations is unknown, their frequency was negligible. Thus, mtDNA heteroplasmic variants would not have significantly influenced our results.

5. Conclusions

The present results indicate that inherited mtDNA common polymorphisms must not be single major cause of AD but the rare variants detected in the protein-coding-region may have protective effect for high-risk population carrying the APOE e4 allele. This suggests one possibility that inherited mtDNA feature would relate in synaptic function rather than in amyloid protein processing directly. Furthermore, our results raised the possibility that the 961T>C causing a poly-C stretch at 956–965 and the 856T>G variant might be the risk for AD. Further investigations along these lines will be important for understanding the pathogenesis of AD and the associated defect in mitochondrial energy production.

Web resources

Further information on mtDNA is available at Mitomap: http://www.mitomap.org/ and mtSNP database: http://www.mtsnp.tmig.or.jp/mtsnp/index.shtml.

Acknowledgements

We thank Dr. Tsutomu Suzuki for helpful suggestion. This work was supported by grants from the Organization for Pharmaceutical Safety and Research (MPJ-2) and from the Institute of Biomedical Innovation (05-41).

Appendix A. Supplementary material

Supplementary data associated with this article can be found, in the online version, at doi:10.1016/j.mito.2009.08.008.

References

Achilli, A., Rengo, C., Battaglia, V., et al., 2005. Saami and Berbers – an unexpected mitochondrial DNA link. Am. J. Hum. Genet. 76, 883–886.
Akanuma, J., Muraki, K., Komaki, H., Nonaka, I., Goto, Y., 2000. Two pathogenic point mutations exist in the authentic mitochondrial genome, not in the nuclear pseudogene. J. Hum. Genet. 45, 337–341.
Asada, T., Motonaga, T., Yamagata, Z., Uno, M., Takahashi, K., 2000. Associations between retrospectively recalled napping behavior and later development of Alzheimer's disease, association with APOE genotypes. Sleep 23, 629–634.
Asari, M., Tan, Y., Watanabe, S., Shimizu, K., Shiono, H., 2007. Effect of length variations at nucleotide positions 303–315 in human mitochondrial DNA on transcription termination. Biochem. Biophys. Res. Commun. 361, 641–644.